Cell Reports

Report

Sh3rf2 Haploinsufficiency Leads to Unilateral Neuronal Development Deficits and Autistic-Like Behaviors in Mice

Graphical Abstract

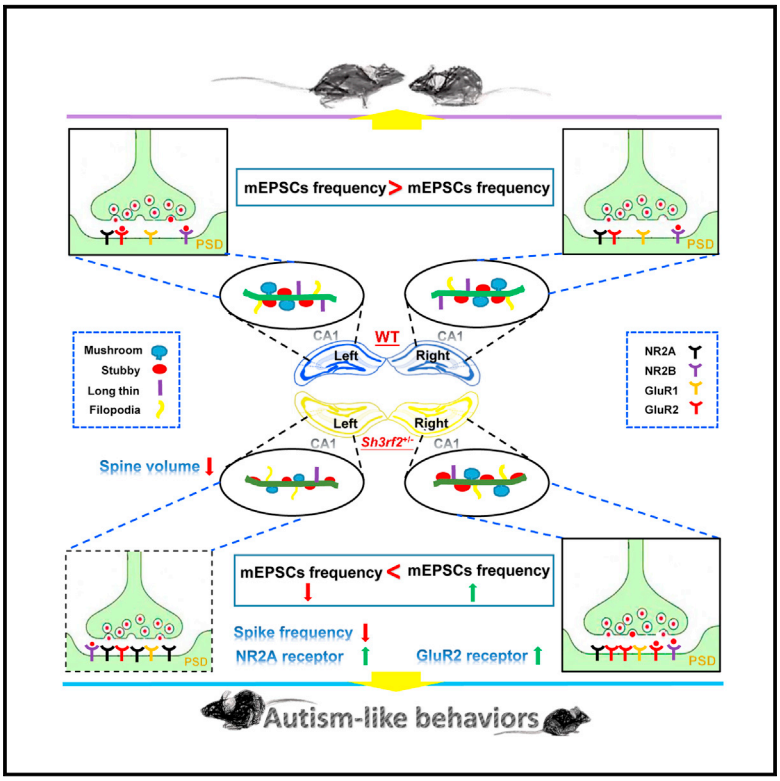

Highlights

- Sh3rf2 is necessary for dendritic spine development and synaptogenesis
- *Sh3rf2* haploinsufficiency leads to autistic-like behaviors in mice
- Disturbances in the hippocampal function of the heterozygote were selectively unilateral

Authors

Shuo Wang, Ningdong Tan, Xingliang Zhu, Minghui Yao, Yaqing Wang, Xiaohui Zhang, Zhiheng Xu

Correspondence

xhzhang@bnu.edu.cn (X.Z.), zhxu@genetics.ac.cn (Z.X.)

In Brief

Wang et al. find that *Sh3rf2* is important for neuron development and that *Sh3rf2* haploinsufficiency in mice results in typical ASD-like behaviors, as well as selective unilateral disturbances in hippocampal dendritic spine development, composition of glutamatergic receptor subunits, and excitatory synaptic transmission.

Wang et al., 2018, Cell Reports *25*, 2963–2971
December 11, 2018
https://doi.org/10.1016/j.celrep.2018.11.044

CellPress

Cell Reports
Report

Sh3rf2 Haploinsufficiency Leads to Unilateral Neuronal Development Deficits and Autistic-Like Behaviors in Mice

Shuo Wang,[1,3,6] Ningdong Tan,[2,6] Xingliang Zhu,[1,3] Minghui Yao,[1] Yaqing Wang,[1] Xiaohui Zhang,[2,*] and Zhiheng Xu[1,4,5,*]
[1]State Key Laboratory of Molecular Developmental Biology, CAS Center for Excellence in Brain Science and Intelligence Technology, Institute of Genetics and Developmental Biology, Chinese Academy of Sciences, Beijing 100101, China
[2]State Key Laboratory of Cognitive Neuroscience and Learning, IDG/McGovern Institute for Brain Research, Beijing Normal University, Beijing 100875, China
[3]University of Chinese Academy of Sciences, Beijing 100101, China
[4]Parkinson's Disease Center, Beijing Institute for Brain Disorders, Beijing 100101, China
[5]Lead Contact
[6]These authors contributed equally
*Correspondence: xhzhang@bnu.edu.cn (X.Z.), zhxu@genetics.ac.cn (Z.X.)
https://doi.org/10.1016/j.celrep.2018.11.044

SUMMARY

Autism spectrum disorders (ASDs) include a variety of developmental brain disorders with clinical findings implicating the dysfunction of the left hemisphere. Here, we generate mice lacking one copy of *Sh3rf2*, which was detected in ASD patients, to determine whether Sh3rf2 is involved in brain development and whether mutation of *SH3RF2* is causative for ASD and the mechanisms linking it to ASD traits. We find that mice with *Sh3rf2* haploinsufficiency display significant deficits in social interaction and communication, as well as stereotyped or repetitive behaviors and hyperactivity and seizures. Disturbances in hippocampal dendritic spine development, aberrant composition of glutamatergic receptor subunits, and abnormal excitatory synaptic transmission were detected in heterozygous mutants. Remarkably, these defects are selectively unilateral. Our results support a notion that *Sh3rf2* haploinsufficiency is a highly penetrant risk factor for ASD, with disease pathogenesis most likely resulting from deficits in synaptic function in the left hemisphere of the brain.

INTRODUCTION

Autism spectrum disorder (ASD) is a childhood-onset neuropsychiatric disorder that is characterized by deficits in social communication and social interactions, as well as stereotyped, repetitive behaviors and/or restricted interests (American Psychiatric Association, 2013). Global attention has been drawn to ASD due to its apparently growing prevalence, from a global prevalence of 62 in 10,000 to as high as 1 in 68 in the United States (Yu et al., 2017).

ASD has been recognized as a complex brain developmental disorder (Miles, 2011). Although the right and left brain hemispheres appear as mirror images on first impression, many reports indicate fundamental differences in the processing of information between the hemispheres, such as language in the left hemisphere (Concha et al., 2012; Bray, 2016). Failure to develop normal language comprehension and language leftward functional asymmetry is an early sign of autism (Eyler et al., 2012). Accordingly, left hemisphere dysfunction is often seen in autistic patients (Ben Bashat et al., 2007; El-Badri and Lewis, 1993; Gomot et al., 2002; McAlonan et al., 2009; Roberts et al., 2014).

ASD is a heterogeneous disorder with a complex genetic basis; the genetic contribution to pathophysiology is challenging to explore because of incomplete penetrance, a large number of susceptibility genes, and complex gene-environment interactions (de la Torre-Ubieta et al., 2016; Sztainberg and Zoghbi, 2016). Until now, only a few ASD loci have been confirmed in animal models (Bourgeron, 2015). Therefore, investigation of the biological function of these risk factors in brain circuitry formation and maintenance at the molecular, cellular, and behavioral levels would shed light on the disease etiology and targeted strategies for drug development.

Excitatory synapses located on dendritic spines and dendritic spine size directly correlate with excitatory synapse strength (Bonhoeffer and Yuste, 2002). Dysregulated synaptic development, properties, and plasticity were hypothesized to underlie altered neuronal function in complex neuropsychiatric disorders, such as ASD and schizophrenia (Ebert and Greenberg, 2013; Forrest et al., 2018; Zhang et al., 2016).

Gau et al. (2012) reported two novel private copy-number variants in a male patient diagnosed with typical autistic disorder. *SH3RF2*, a gene found in 1.8-Mb microdeletion at 5q32, was transmitted from his father with mild autistic symptoms. All of the genes in the 1.8-Mb microdeletion at 5q32, except *SH3RF2*, have been studied in gene knockout mice with no autistic behaviors reported. Furthermore, both insertion and deletion mutations, as well as nine single-nucleotide variants in *SH3RF2* were recently found in 12 ASD patients (Yuen et al., 2017). *SH3RF2* is therefore a potential candidate gene for ASD.

SH3RF2 (also known as POSHER), a putative ubiquitin E3 ligase, belongs to the SH3RF (SH3 domain containing RING

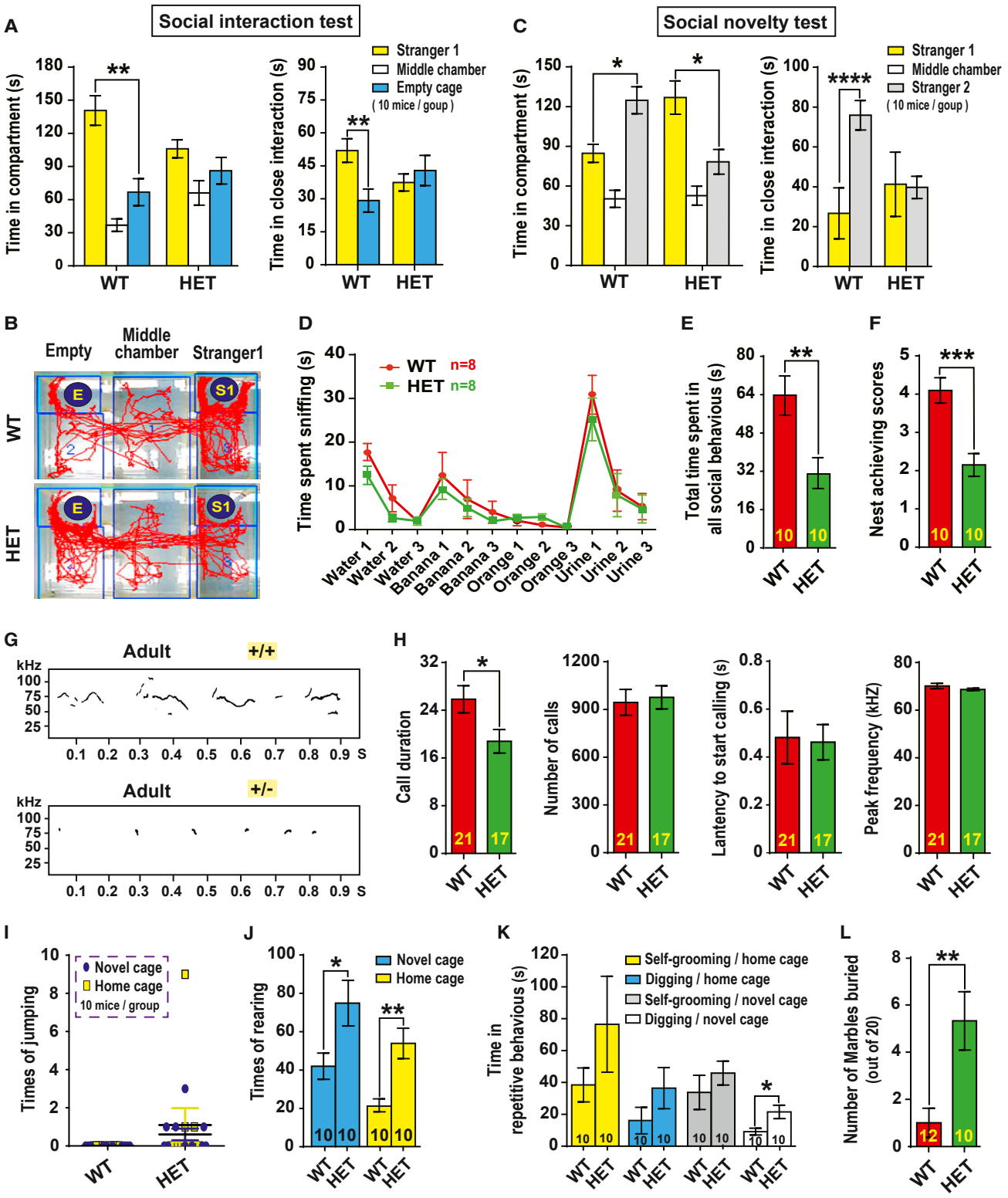

Figure 1. *Sh3rf2*$^{+/-}$ Mice Exhibit Various ASD-Like Behaviors

(A–C) Impaired social interaction of *Sh3rf2*$^{+/-}$ mice in the three-chamber assay.

(A) In the social interaction test, *Sh3rf2*$^{+/-}$ mice spent less time in the chamber containing the social partner (stranger 1) and more time in the chamber containing the empty cage when compared with controls.

(legend continued on next page)

finger protein) family of proteins (Wilhelm et al., 2012) and contains three SH3 domains, as well as a Ring finger domain. We have previously shown that SH3RF2 promotes the survival of PC12 cells through the degradation of another SH3RF family member, POSH (SH3RF1) (Wilhelm et al., 2012). In addition, SH3RF2 is overexpressed in cancer cell lines and may function as an oncogene (Kim et al., 2014). However, the physiological role of SH3RF2 and its underlying mechanisms remain unknown.

To investigate the biological function of SH3RF2 in brain and its relevance to ASD, we generated *Sh3rf2* knockout mice and found that *Sh3rf2* haploinsufficiency leads to unilateral disturbance of hippocampal function and typical ASD-like behaviors.

RESULTS

Generation of *Sh3rf2* Knockout Mice

To disrupt *Sh3rf2*, exon 1 was replaced by a *lacZ* expression cassette (Figure S1A). Accurate targeting was confirmed by PCR and Southern blot (Figures S1B–S1D). Evident decreased expression of *Sh3rf2*, but not other SH3RF family members, *Sh3rf1* (*POSH*) and *Sh3rf3*, was confirmed by qRT-PCR analyses (Figures S1E–S1G).

When mating heterozygous mice, $Sh3rf2^{-/-}$ mutants were born at decreased birth rates [male (wild-type [WT]:heterozygote [HET]:homozygote [HOM], 1:1.91:0.69); female (WT:HET:HOM, 1:2.13:0.83)]. Deletion of either one or both copies of *Sh3rf2* resulted in reduced growth in some male mice after birth (Figure S1H), with 10.8% male HETs and 12.5% male HOMs that died during their postnatal growth (Figure S1I). However, most of them grew normally. ASD is a mostly heterogeneous human disorder (Yuen et al., 2017; Rosti et al., 2014), and there are many examples of haploinsufficiency in mice leading to ASD, including SHANK3, CHD8, or NUAK1 (Bozdagi et al., 2010; Courchet et al., 2018; Katayama et al., 2016). Moreover, only one allele of *Sh3rf2* was deleted in the reported patient and his father (Gau et al., 2012). Therefore, we used male WT and $Sh3rf2^{+/-}$ mice matched by weight in the following experiments (Figure S1J). These $Sh3rf2^{+/-}$ mice showed normal brain morphology (including the hippocampus) (Figure S1K).

$Sh3rf2^{+/-}$ Mice Display Deficits in Both Sociability and Social Novelty Preference, and Social Communication

Deficits in social interaction are the most recognizable manifestation of autistic behaviors (Peça et al., 2011; Won et al., 2012). $Sh3rf2^{+/-}$ and WT mice were subjected to a three-chamber social interaction assay to test the voluntary initiation of social interaction and the ability to discriminate social novelty (Moy et al., 2004; Won et al., 2012). In the social interaction test, WT mice preferred to explore the novel social partner (stranger 1) more frequently than $Sh3rf2^{+/-}$ mice; these social interaction performances were measured by observing both the time spent in the compartments and also close interaction (Figures 1A and 1B). Next, when another novel mouse (stranger 2) was introduced into the previously empty cage (social novelty test), $Sh3rf2^{+/-}$ mice did not show a preference to explore stranger 2 compared with stranger 1 (Figure 1C), in contrast to WT mice, thus indicating impaired social novelty recognition in $Sh3rf2^{+/-}$ mice. The possibility of olfactory dysfunction on social interaction was excluded as $Sh3rf2^{+/-}$ mice had normal responses to both social cues and non-social cues (Figure 1D). During a free dyadic encounter, $Sh3rf2^{+/-}$ mice also displayed reduced social interaction with the stimulus mice (Figure 1E). Several $Sh3rf2^{+/-}$ mice even ran away from the novel mice (Video S1). In autism mouse models, impaired nest building is often correlated with impaired social behaviors (Jirkof, 2014). We found that $Sh3rf2^{+/-}$ mice had a substantially decreased nesting score in the nest-building assay compared with WT mice (Figure 1F).

To determine whether $Sh3rf2^{+/-}$ mice were deficient in social communication, we performed an ultrasonic vocalizations (USVs) test, which is used to inspect the social communication of mice (Scattoni et al., 2009). When postnatal day 8 (P8) male pups were isolated from their dams and littermates, the durations of isolation-induced USV (call) emitted by $Sh3rf2^{+/-}$ pups were significantly shorter than in WT pups (Figures S2A and S2B). For adult male mice, when allowed to interact with a novel WT female mouse, $Sh3rf2^{+/-}$ mice emitted USVs that were significantly shorter in duration (Figures 1G and 1H).

The above results indicate that $Sh3rf2^{+/-}$ mice display abnormal social interaction and communication. Of note, all genotypes were nurtured by $Sh3rf2^{+/-}$ dams, but genotypes performed differently in social behaviors, indicating a genetic origin for the abnormal social behaviors in $Sh3rf2^{+/-}$ mice.

$Sh3rf2^{+/-}$ Mice Exhibit Stereotyped, Repetitive Behaviors, and Other Autism-Associated Abnormalities

We noticed that many male mutant mice displayed hyperactive behaviors in their home cages, for example, continuous jumping or fighting with littermates (Video S2); also, when kept alone in home cages or novel cages without cage lids, $Sh3rf2^{+/-}$ mice jumped more frequently (Figure 1I), which was combined with significantly increased rearing behaviors (Figures 1J and S2C). Although repetitive self-grooming and digging were reported in

(B) Representative tracks of the two groups in the "stranger 1 – empty" trials.
(C) In the social novelty test, $Sh3rf2^{+/-}$ mice did not display a preference for the novel social partner (stranger 2) and spent more time in the chamber containing stranger 1.
(D) $Sh3rf2^{+/-}$ mice have normal olfactory function.
(E) Impaired social interaction of $Sh3rf2^{+/-}$ mice in the free dyadic social interaction assay.
(F) Impaired nesting behavior in $Sh3rf2^{+/-}$ mice.
(G and H) Impaired social communication by ultrasonic vocalizations (USVs) in adult $Sh3rf2^{+/-}$ mice. USVs examples in adult male mice (G) and changes in courtship USVs in adult male $Sh3rf2^{+/-}$ mice (H) are shown.
(I–L) $Sh3rf2^{+/-}$ mice exhibit stereotypical behaviors. $Sh3rf2^{+/-}$ mice showed enhanced jumping (I). $Sh3rf2^{+/-}$ mice spent more time in rearing behaviors than WT mice, either in their home cage or in a novel cage (J). $Sh3rf2^{+/-}$ mice spent more time digging than WT mice in the novel cage (K). $Sh3rf2^{+/-}$ mice bury significantly more marbles than wild-type mice (L). HET, heterozygote; WT, wild-type; $^*p < 0.05$, $^{**}p < 0.01$, $^{***}p < 0.001$; unpaired t test for (A), (C)–(F), and (H)–(L); all data are presented as means ± SEM.

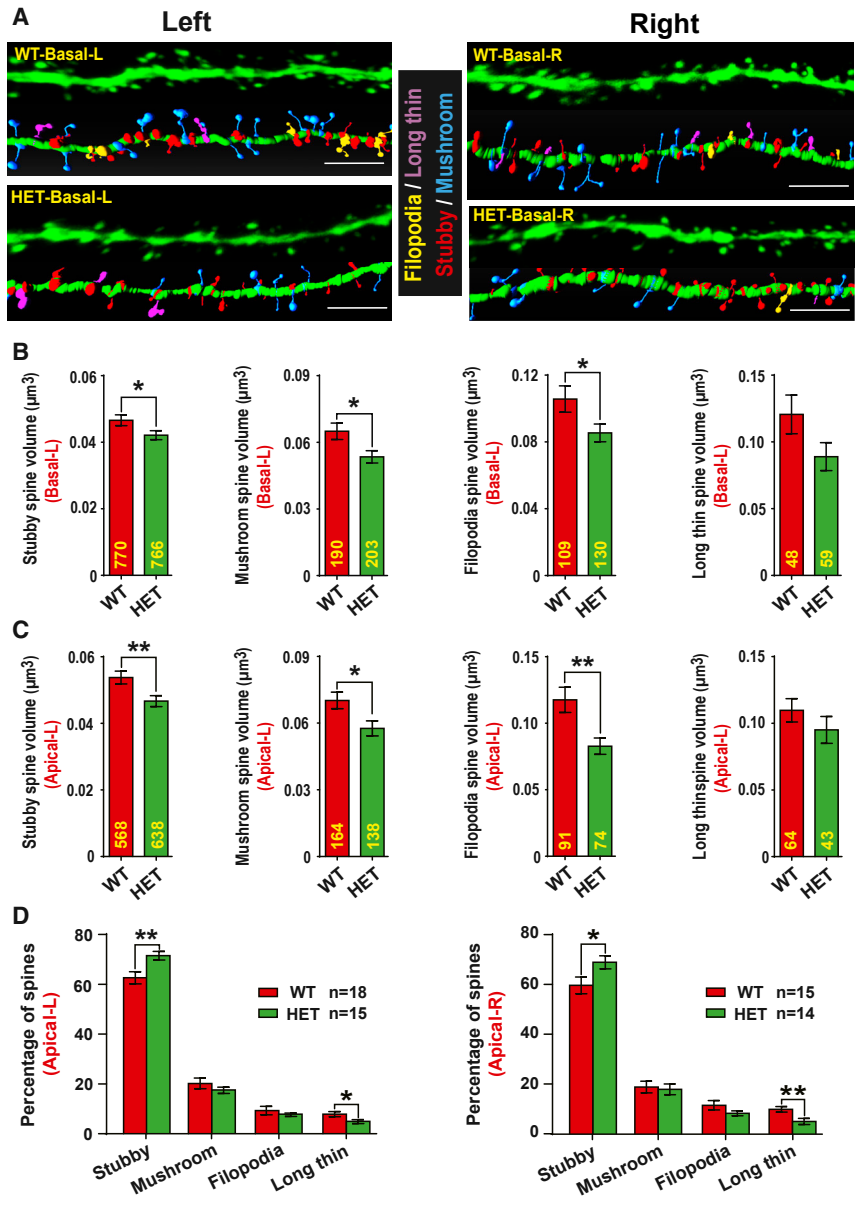

Figure 2. Reduced Dendritic Spine Volume in CA1 PNs in the Left Hippocampus of *Sh3rf2*$^{+/-}$ Mice

(A) Confocal microscopy images of dendritic spines from Thy1-GFPm-labeled secondary basal dendrites of PNs in the CA1 region of the hippocampus (top). Three-dimensional reconstruction of the complete morphology of each dendritic spine shown (bottom). dendrite, green; mushroom spines, blue; stubby spines, red; long thin spines, purple; filopodia spines, yellow. Scale bar: 4 μm.

(B) Dendritic spine volume of the secondary basal dendrites in the left hippocampus: *Sh3rf2*$^{+/-}$ mice displayed decreased volume in different spines including mushroom, stubby, and filopodia spines; n = 23 dendrites (WT), n = 19 dendrites (HET).

(C) Dendritic spine volume of the secondary apical dendrites in the left hippocampus: *Sh3rf2*$^{+/-}$ mice displayed reduced volume in different spines including mushroom, stubby, and filopodia spines; n = 18 dendrites (WT), n = 15 dendrites (HET).

(D) Percentages of spine types in secondary apical dendrites; *Sh3rf2*$^{+/-}$ mice displayed increased percentages of stubby spines and decreased percentages of long thin spines in the bilateral hippocampus. L, left hippocampus; R, right hippocampus; HET, heterozygote; WT, wild-type; n = 6 mice/8 weeks (each group); *p < 0.05, **p < 0.01; unpaired t test for (B)–(D); all data are presented as means ± SEM.

several mouse ASD models (Peça et al., 2011; Won et al., 2012), we observe increased but not significant repetitive grooming in *Sh3rf2*$^{+/-}$ mice (Figure 1K); however, *Sh3rf2*$^{+/-}$ mice showed a significant increase of digging behavior in novel cages (Figure 1K).

The marble-burying test was adopted to study repetitive and compulsive-like behaviors (Angoa-Pérez et al., 2013). We found that *Sh3rf2*$^{+/-}$ mice buried significantly more marbles than controls (Figures 1L and S2D), indicating that they dig compulsively in a novel environment.

In addition to the typical ASD-like behaviors, *Sh3rf2*$^{+/-}$ mice exhibited other autism-associated abnormalities. Spontaneous seizures were observed in young *Sh3rf2*$^{+/-}$ mice, and several of these seizures were lethal (Video S3).

Asymmetric Morphological Changes in *Sh3rf2*$^{+/-}$ Hippocampal Pyramidal Neurons

Dysregulated synaptic development has been hypothesized to underlie altered neuronal function in ASD (Ebert and Greenberg, 2013). As left hemisphere (including the hippocampus) dysfunction is often found in autism patients, we investigated whether *Sh3rf2* plays a role in hippocampal dendritic spine development and synaptogenesis, both in the left and right hippocampi, respectively. We first inspected in detail the morphology of dendritic spines in Thy1-GFPm-labeled cornu ammonis (CA) 1 pyramidal neurons (PNs) (Figure 2A). Interestingly, in *Sh3rf2*$^{+/-}$ mice, we found decreased spine volumes in secondary basal dendrites of left hippocampal CA1 PNs, but not in right hemisphere CA1 PNs (Figures 2B and S3A). This decreased volume was evident in different spines including mushroom, stubby, and filopodia spines. In addition, no difference in spine density or ratios of different spine types (Figures S3B and S3C) was detected.

Similarly, volumes of these three types of spines decreased evidently in apical dendrites of the left hippocampus of *Sh3rf2*$^{+/-}$ mice (Figure 2C), while only reduced filopodia spine volumes were evident in the right hippocampus (Figure S3D). *Sh3rf2*$^{+/-}$ mice also displayed an increased ratio of stubby spines but a decreased ratio of long thin spines in the bilateral

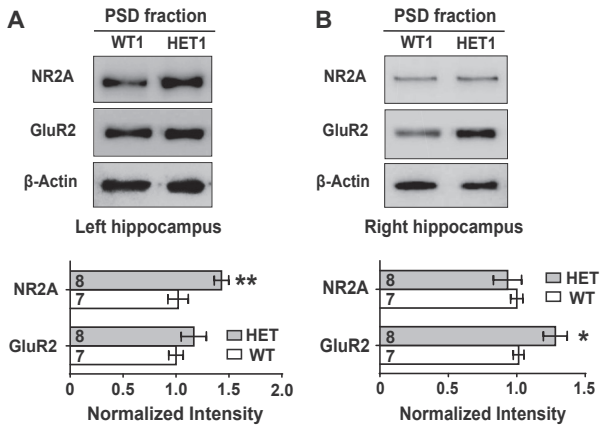

Figure 3. *Sh3rf2*$^{+/-}$ Mice Display Hemisphere-Asymmetric Changes in Hippocampal PSD Fractions

(A) Protein levels of glutamate receptor NR2A subunits were increased in PSD fractions from the left hippocampus of *Sh3rf2*$^{+/-}$ mice.

(B) Protein levels of glutamate receptor GluR2 (also known as GluA2) subunits were increased in PSD fractions from the right hippocampus of *Sh3rf2*$^{+/-}$ mice. β-Actin was used as a loading control normalized to wild-type levels. HET, heterozygote; WT, wild-type; *$p < 0.05$, **$p < 0.01$; unpaired t test for (A) and (B); data are presented as means ± SEM.

hippocampus (Figure 2D), indicating an increase in the density of mature spine. Also, no difference in spine density was found in apical dendrites (Figure S3E).

To confirm that Sh3rf2 is necessary for spine development, we isolated hippocampal neurons from embryonic day 18 (~E18) WT and *Sh3rf2*$^{+/-}$ mice and cultured them for 11 days before overexpression of *Sh3rf2*. Nine days later, HET PNs displayed a decreased ratio of stubby spine but an increased ratio of filopodia spine in the secondary dendrites (Figures S3F and S3G), as well as decreased spine density and volume (Figures S3H–S3L). Those abnormalities can be rescued by expression of Sh3rf2 (Figures S3G–S3L).

Hemisphere-Asymmetric Changes in Glutamate Receptor Subunits in PSD Fractions of the Hippocampus in *Sh3rf2*$^{+/-}$ Mice

To determine whether the hemisphere-asymmetric effect on dendritic spine volume might affect receptors at the postsynaptic density (PSD), we purified PSDs from the hippocampi of WT and *Sh3rf2*$^{+/-}$ mice. Compared with WT mice, increased NR2A and GluR2 in the respective left and right hippocampi of *Sh3rf2*$^{+/-}$ mice were detected (Figures 3A and 3B), although no significant changes in GluR1 or NR2B levels were evident (Figures S4A and S4B). These results suggest an asymmetric enrichment of NMDA and AMPA receptors in the left and right hippocampi, respectively.

Altered Membrane Properties of Hippocampal Neurons in *Sh3rf2*$^{+/-}$ Mice

The hemisphere-asymmetric effects on dendritic spines and glutamate receptors led us to explore whether neuronal or synaptic functions are affected. We inspected the membrane excitability and excitatory synaptic transmission of hippocampal CA1 PNs in acute hippocampal slices prepared from the left or right hemispheres, respectively, using whole-cell recording. We first examined the passive membrane property and intrinsic excitability of CA1 PNs by intracellular injection of step currents in the current-clamp mode (Figure 4A). All recorded CA1 PNs showed similar typical accommodating spiking patterns. When recordings from PNs in bilateral hippocampal slices from WT mice and *Sh3rf2*$^{+/-}$ mice were compared, *Sh3rf2*$^{+/-}$ neurons exhibited smaller after-hyperpolarization (AHP) (Table S1). However, when PNs in the left and right hippocampi of each genotype were compared separately, we found prominent differences in several membrane parameters (Table S1). For instance, in the right hippocampus, *Sh3rf2*$^{+/-}$ neurons had significantly higher membrane resistance, smaller capacitance, and lower AHP than WT neurons. In contrast, in the left hippocampus, *Sh3rf2*$^{+/-}$ and WT neurons showed no difference in membrane parameters (Table S1). Moreover, when the input-output (I/O) curves were compared (Figures 4B and S4D), in the left hippocampus, *Sh3rf2*$^{+/-}$ neurons had significantly lower spike frequency but had no significant difference in the average I-O slope or rheobase (Table S1).

Altered AMPA Receptor-Mediated Excitatory Synaptic Inputs in *Sh3rf2*$^{+/-}$ Neurons

We next examined whether there might be altered excitatory synaptic inputs in *Sh3rf2*$^{+/-}$ CA1 PNs, by recording miniature excitatory postsynaptic currents (mEPSCs) (Figure 4C). When all PNs recorded in both the left and right hippocampi were pooled, we did not observe any significant difference in the inter-event interval (or frequency) or the amplitude of mEPSCs between *Sh3rf2*$^{+/-}$ and WT PNs (Figure S4E). However, when recorded PNs were grouped for the left and right hippocampi, respectively, we found *Sh3rf2*$^{+/-}$ neurons showed a reduced frequency in the left hippocampus (Figure 4D) but an increased frequency in the right hippocampus (Figure 4E), in comparison with that of WT. However, when the left and right hippocampi were compared for individual genotypes, WT PNs showed relatively higher mEPSC frequency in the left hippocampus, while *Sh3rf2*$^{+/-}$ PNs had higher mEPSC frequency in the right hippocampus (Figures 4F and 4G), indicating an opposite change in the asymmetry of mEPSC events between WT and *Sh3rf2*$^{+/-}$ mice. Taken together, the results suggest that *Sh3rf2*$^{+/-}$ mice show significant alterations in excitatory synaptic transmission in the hippocampal CA1 area, and interestingly the alterations are asymmetric between the bilateral hippocampi.

DISCUSSION

Establishing causality between genetic mutations, synaptic changes, circuit dysfunctions, and abnormal behaviors is one of the greatest advantages of using mouse models that can potentially aid us in our understanding of neuropsychiatric diseases (Kaiser et al., 2017; Rothwell et al., 2014). In the present study, we provide strong evidence to support a critical role for *Sh3rf2* in the expression of structural abnormalities and autism-like behaviors. Our comprehensive set of behavioral analyses revealed that mice with a *Sh3rf2* haploinsufficiency exhibit several impairments observed in autism patients, including

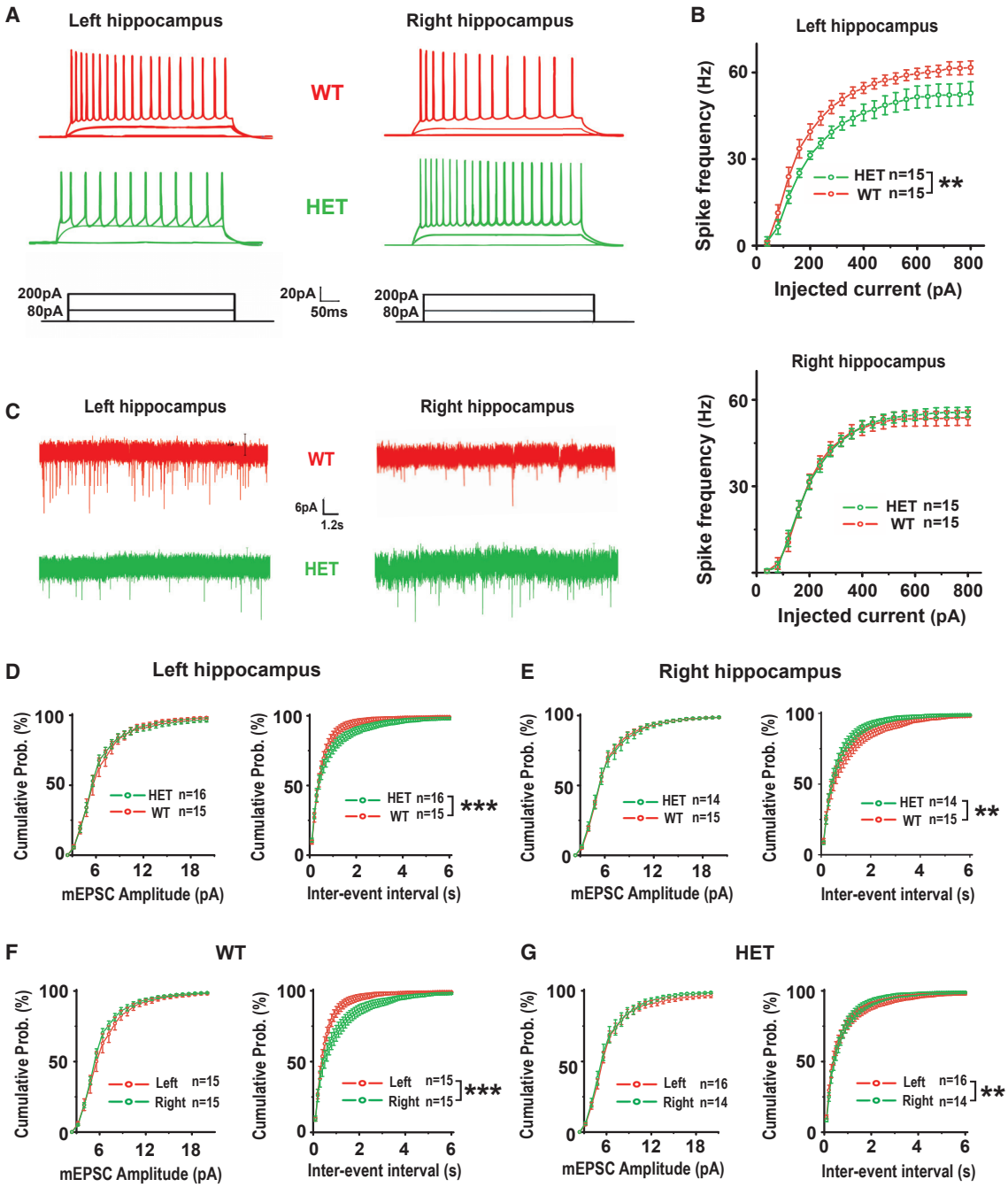

Figure 4. Unilateral Alterations of Neuronal and Synaptic Functions in the Hippocampus of *Sh3rf2*$^{+/-}$ Mice

(A and B) Unilateral altered membrane properties.

(A) Example recording traces depicting action potential firing of hippocampal CA1 PNs in response to step depolarizing currents in slices from WT and *Sh3rf2*$^{+/-}$ mice.

(B) Plots of evoked spike rates versus current magnitudes (I/O curve) of PNs in the left (upper) and right (bottom) hippocampus from WT and *Sh3rf2*$^{+/-}$ mice, respectively. WT: n = 15 cells in 2 mice; HET: n = 15 cells in 5 mice.

(C–G) Differential alterations of mEPSCs in the left and right hippocampi.

(C) Example recording traces of mEPSCs recorded in CA1 PNs from the left or right hippocampal slices of WT and *Sh3rf2*$^{+/-}$ mice, respectively.

(D and E) Cumulative distributions of the mEPSC amplitude (left) or the inter-event interval (right) in the left (D) or right (E) hippocampal slices of WT and *Sh3rf2*$^{+/-}$ mice; n(WT): left, from 6 mice, and right, from 4 mice; n(HET): left, from 4 mice, and right, from 5 mice.

(F and G) Similar to (D) and (E) except the same set of data are polled according to the genotypes showing comparisons between the left and right hippocampus in WT (F) or *Sh3rf2*$^{+/-}$ mice (G). **p < 0.01, ***p < 0.001, tested by Kolmogorov-Smirnov test; all data are presented as means ± SEM.

deficits in social interactions and communication, repetitive behaviors, and seizures. More importantly, our findings indicate a selectively unilateral disturbance of hippocampal dendrite development, aberrant composition of glutamatergic receptors, and abnormal electrophysiology in *Sh3rf2*$^{+/-}$ mice, and that these disturbances may contribute to autism-like behaviors.

Dysfunction of left hemisphere has been identified in many autism patients (El-Badri and Lewis, 1993; Gomot et al., 2002; Roberts et al., 2014). We found that *Sh3rf2* plays a role in hippocampal dendritic spine development and synaptogenesis. Interestingly, in *Sh3rf2*$^{+/-}$ mice, there was significantly decreased secondary dendritic spine volume in CA1 PNs of the left, but not the right hippocampus—with exception of immature filopodia spine in the apical dendrites. The size of dendritic spines correlates with the strength of excitatory synapses (Bonhoeffer and Yuste, 2002). We found that, in the left dorsal CA1 region, *Sh3rf2*$^{+/-}$ PNs showed a decreased rate in spikes in response to depolarization inputs, as well as a lower frequency of excitatory synaptic inputs, indicating a relatively reduced capacity in hippocampal information transfer.

Intriguingly, elevated NR2A protein levels were found in HETs, while NR2B remained unchanged. Increased NR2A:NR2B ratios compressed long-term depression (LTD) ranges and reduced long-term memory (Cui et al., 2013). Induction of LTD by low-frequency stimulation was accompanied by a marked shrinkage of spines, which was mediated by NMDA receptor activation (Zhou et al., 2004). Therefore, NR2A upregulation and NR2A-induced spine shrinkage may contribute to decreased spine volume in *Sh3rf2*$^{+/-}$ mice. Moreover, overexpression of NR2A subunit in forebrain, including the hippocampus, is known to impair both long-term social recognition and non-social olfactory memory (Jacobs and Tsien, 2014). Thus, an increase in NR2A subunits in the left hippocampus of *Sh3rf2*$^{+/-}$ mice may contribute to impairments in social interaction.

Although we provide evidence that selectively unilateral disturbance of dendritic spine development in the left hippocampus contributes to dysfunctions that may cause autism-like behaviors in *Sh3rf2*$^{+/-}$ mice, we noticed that *Sh3rf2* haploinsufficiency led to an increased ratio of mature stubby spines in both left and right hippocampi and a higher level of GluR2 in PSD fractions of the right hippocampus, in addition to elevated intrinsic excitability, enhanced GluR2-mediated synaptic transmission, and increased functional synapses. Additional mechanistic studies are warranted to investigate whether *Sh3rf2*$^{+/-}$ mice have enhanced learning and memory, similar to autistic savants (patients with special or unusual talents).

Together, our results show a critical contribution of *Sh3rf2* haploinsufficiency in distinct physiological, neuroanatomical, and behavioral phenotypes. We observed specific abnormalities associated with neuronal development in the hippocampus that, if recapitulated throughout the brain, could help to explain the dysregulation of neural circuits and the subsequent effects on distinct types of behaviors. *Sh3rf2*$^{+/-}$ mice exhibited key structural and synaptic plasticity deficits in neurons and also exhibited behavioral impairments, which spanned multiple symptomatic domains related to ASD. Considering the emerging focus on research domain criteria in the clinical field, it will be important to map genetic risk to functional domains at the cellular, systems, and behavioral levels to identify points of convergence and divergence in biological pathways associated with the etiology of psychiatric disease.

Sh3rf2 is unique among the few risk genes that have been studied so far in that its haploinsufficiency, as in most ASD patients, leads to phenotypes ranging from synaptic dysfunction to behavioral phenotypes that are associated with multiple symptomatic domains, suggesting it may be a core gene that aligns with many features of ASD. *Sh3rf2*$^{+/-}$ mice may therefore serve as a valuable animal model for ASD research, amenable to targeted investigations of mechanistic postulations of neurodevelopmental dysregulation.

STAR★METHODS

Detailed methods are provided in the online version of this paper and include the following:

- KEY RESOURCES TABLE
- CONTACT FOR REAGENT AND RESOURCE SHARING
- EXPERIMENTAL MODEL AND SUBJECT DETAILS
  - Animal studies
- METHOD DETAILS
  - Generation of Sh3rf2 conventional knockout mice
  - Behavioral tests
  - Three-chamber social interaction assay
  - Free dyadic social interaction
  - Nest building assay
  - Olfactory function test
  - Ultrasonic vocalization in isolation pulps
  - Interaction-induced ultrasonic vocalization in adult mice
  - Grooming, digging and jumping in novel cage and home cage
  - Rearing in novel cage and home cage
  - Marble Burying Test
  - Analysis of dendritic arborization and spine morphology
  - Histological and immunofluorescent staining of Mouse Brain Sections
  - Biochemical analyses
  - RNA extraction, cDNA synthesis and quantitative real-time PCR
  - Primary hippocampal cultures and transfection of primary neurons
  - Electrophysiology
- QUANTIFICATION AND STATISTICAL ANALYSIS

SUPPLEMENTAL INFORMATION

Supplemental Information includes four figures, one table, and three videos and can be found with this article online at https://doi.org/10.1016/j.celrep.2018.11.044.

ACKNOWLEDGMENTS

We thank Drs. X. Yu, G. Feng, and Y. Jiang for their constructive advice, and Dr. Yi Zuo for providing Thy1-*GFPm* mice. This work was supported by the Strategic Priority Research Program and Innovation Program of the Chinese

Academy of Sciences (XDBS1020100, XDA16010306, QYZDJ-SSW-SMC007, and GJHZ1827), the National Natural Science Foundation of China (31730108/31430037/31471132/31571038), Shanghai Brain-Intelligence Project from STCSM (16JC1420500) and Beijing Brain Project (Z161100002616004), and the Interdisciplinary Research Funds of Beijing Normal University.

AUTHOR CONTRIBUTIONS

S.W., Z.X., and X. Zhang designed the experiments. N.T. performed electrophysiology experiments. S.W. performed most of the other experiments. X. Zhu, M.Y., and Y.W. performed some biochemical and animal experiments. S.W. and N.T. prepared manuscript drafts. Z.X. and X. Zhang edited the paper.

DECLARATION OF INTERESTS

The authors declare no competing interests.

Received: May 1, 2018
Revised: September 20, 2018
Accepted: November 9, 2018
Published: December 11, 2018

REFERENCES

Angoa-Pérez, M., Kane, M.J., Briggs, D.I., Francescutti, D.M., and Kuhn, D.M. (2013). Marble burying and nestlet shredding as tests of repetitive, compulsive-like behaviors in mice. J. Vis. Exp. *2013*, 50978.

American Psychiatric Association (2013). Diagnostic and Statistical Manual of Mental Disorders, Fifth Edition (American Psychiatric Association).

Ben Bashat, D., Kronfeld-Duenias, V., Zachor, D.A., Ekstein, P.M., Hendler, T., Tarrasch, R., Even, A., Levy, Y., and Ben Sira, L. (2007). Accelerated maturation of white matter in young children with autism: a high b value DWI study. Neuroimage *37*, 40–47.

Bonhoeffer, T., and Yuste, R. (2002). Spine motility. Phenomenology, mechanisms, and function. Neuron *35*, 1019–1027.

Bourgeron, T. (2015). From the genetic architecture to synaptic plasticity in autism spectrum disorder. Nat. Rev. Neurosci. *16*, 551–563.

Bozdagi, O., Sakurai, T., Papapetrou, D., Wang, X., Dickstein, D.L., Takahashi, N., Kajiwara, Y., Yang, M., Katz, A.M., Scattoni, M.L., et al. (2010). Haploinsufficiency of the autism-associated Shank3 gene leads to deficits in synaptic function, social interaction, and social communication. Mol. Autism *1*, 15.

Bray, N. (2016). Language: mapping meaning. Nat. Rev. Neurosci. *17*, 335.

Concha, M.L., Bianco, I.H., and Wilson, S.W. (2012). Encoding asymmetry within neural circuits. Nat. Rev. Neurosci. *13*, 832–843.

Courchet, V., Roberts, A.J., Meyer-Dilhet, G., Del Carmine, P., Lewis, T.L., Jr., Polleux, F., and Courchet, J. (2018). Haploinsufficiency of autism spectrum disorder candidate gene NUAK1 impairs cortical development and behavior in mice. Nat. Commun. *9*, 4289.

Cui, Z.Z., Feng, R.B., Jacobs, S., Duan, Y.H., Wang, H.M., Cao, X.H., and Tsien, J.Z. (2013). Increased NR2A:NR2B ratio compresses long-term depression range and constrains long-term memory. Sci. Rep. *3*, 1036.

de la Torre-Ubieta, L., Won, H., Stein, J.L., and Geschwind, D.H. (2016). Advancing the understanding of autism disease mechanisms through genetics. Nat. Med. *22*, 345–361.

Deacon, R.M.J. (2006). Assessing nest building in mice. Nat. Protoc. *1*, 1117–1119.

Ebert, D.H., and Greenberg, M.E. (2013). Activity-dependent neuronal signalling and autism spectrum disorder. Nature *493*, 327–337.

El-Badri, S., and Lewis, M. (1993). Left hemisphere and cerebellar damage in Asperger's syndrome. Ir. J. Psychol. Med. *10*, 22–23.

Elias, G.M., Funke, L., Stein, V., Grant, S.G., Bredt, D.S., and Nicoll, R.A. (2006). Synapse-specific and developmentally regulated targeting of AMPA receptors by a family of MAGUK scaffolding proteins. Neuron *52*, 307–320.

Eyler, L.T., Pierce, K., and Courchesne, E. (2012). A failure of left temporal cortex to specialize for language is an early emerging and fundamental property of autism. Brain *135*, 949–960.

Feng, G., Mellor, R.H., Bernstein, M., Keller-Peck, C., Nguyen, Q.T., Wallace, M., Nerbonne, J.M., Lichtman, J.W., and Sanes, J.R. (2000). Imaging neuronal subsets in transgenic mice expressing multiple spectral variants of GFP. Neuron *28*, 41–51.

Feyder, M., Karlsson, R.M., Mathur, P., Lyman, M., Bock, R., Momenan, R., Munasinghe, J., Scattoni, M.L., Ihne, J., Camp, M., et al. (2010). Association of mouse Dlg4 (PSD-95) gene deletion and human DLG4 gene variation with phenotypes relevant to autism spectrum disorders and Williams' syndrome. Am. J. Psychiatry *167*, 1508–1517.

Forrest, M.P., Parnell, E., and Penzes, P. (2018). Dendritic structural plasticity and neuropsychiatric disease. Nat. Rev. Neurosci. *19*, 215–234.

Gau, S.S.F., Liao, H.M., Hong, C.C., Chien, W.H., and Chen, C.H. (2012). Identification of two inherited copy number variants in a male with autism supports two-hit and compound heterozygosity models of autism. Am. J. Med. Genet. B. Neuropsychiatr. Genet. *159B*, 710–717.

Gomot, M., Giard, M.H., Adrien, J.L., Barthelemy, C., and Bruneau, N. (2002). Hypersensitivity to acoustic change in children with autism: electrophysiological evidence of left frontal cortex dysfunctioning. Psychophysiology *39*, 577–584.

He, L.J., Liu, N., Cheng, T.L., Chen, X.J., Li, Y.D., Shu, Y.S., Qiu, Z.L., and Zhang, X.H. (2014). Conditional deletion of Mecp2 in parvalbumin-expressing GABAergic cells results in the absence of critical period plasticity. Nat. Commun. *5*, 5036.

Jacobs, S.A., and Tsien, J.Z. (2014). Overexpression of the NR2A subunit in the forebrain impairs long-term social recognition and non-social olfactory memory. Genes Brain Behav. *13*, 376–384.

Jirkof, P. (2014). Burrowing and nest building behavior as indicators of well-being in mice. J. Neurosci. Methods *234*, 139–146.

Kaiser, T., Zhou, Y., and Feng, G. (2017). Animal models for neuropsychiatric disorders: prospects for circuit intervention. Curr. Opin. Neurobiol. *45*, 59–65.

Katayama, Y., Nishiyama, M., Shoji, H., Ohkawa, Y., Kawamura, A., Sato, T., Suyama, M., Takumi, T., Miyakawa, T., and Nakayama, K.I. (2016). CHD8 haploinsufficiency results in autistic-like phenotypes in mice. Nature *537*, 675–679.

Kim, T.W., Kang, Y.K., Park, Z.Y., Kim, Y.H., Hong, S.W., Oh, S.J., Sohn, H.A., Yang, S.J., Jang, Y.J., Lee, D.C., et al. (2014). SH3RF2 functions as an oncogene by mediating PAK4 protein stability. Carcinogenesis *35*, 624–634.

Li, Y., Xu, J., Liu, Y., Zhu, J., Liu, N., Zeng, W., Huang, N., Rasch, M.J., Jiang, H., Gu, X., et al. (2017). A distinct entorhinal cortex to hippocampal CA1 direct circuit for olfactory associative learning. Nat. Neurosci. *20*, 559–570.

McAlonan, G.M., Cheung, C., Cheung, V., Wong, N., Suckling, J., and Chua, S.E. (2009). Differential effects on white-matter systems in high-functioning autism and Asperger's syndrome. Psychol. Med. *39*, 1885–1893.

Miles, J.H. (2011). Autism spectrum disorders—a genetics review. Genet. Med. *13*, 278–294.

Moy, S.S., Nadler, J.J., Perez, A., Barbaro, R.P., Johns, J.M., Magnuson, T.R., Piven, J., and Crawley, J.N. (2004). Sociability and preference for social novelty in five inbred strains: an approach to assess autistic-like behavior in mice. Genes Brain Behav. *3*, 287–302.

Peça, J., Feliciano, C., Ting, J.T., Wang, W., Wells, M.F., Venkatraman, T.N., Lascola, C.D., Fu, Z., and Feng, G. (2011). Shank3 mutant mice display autistic-like behaviours and striatal dysfunction. Nature *472*, 437–442.

Roberts, T.P., Heiken, K., Zarnow, D., Dell, J., Nagae, L., Blaskey, L., Solot, C., Levy, S.E., Berman, J.I., and Edgar, J.C. (2014). Left hemisphere diffusivity of the arcuate fasciculus: influences of autism spectrum disorder and language impairment. AJNR Am. J. Neuroradiol. *35*, 587–592.

Rosti, R.O., Sadek, A.A., Vaux, K.K., and Gleeson, J.G. (2014). The genetic landscape of autism spectrum disorders. Dev. Med. Child Neurol. *56*, 12–18.

Rothwell, P.E., Fuccillo, M.V., Maxeiner, S., Hayton, S.J., Gokce, O., Lim, B.K., Fowler, S.C., Malenka, R.C., and Südhof, T.C. (2014). Autism-associated neuroligin-3 mutations commonly impair striatal circuits to boost repetitive behaviors. Cell *158*, 198–212.

Scattoni, M.L., Crawley, J., and Ricceri, L. (2009). Ultrasonic vocalizations: a tool for behavioural phenotyping of mouse models of neurodevelopmental disorders. Neurosci. Biobehav. Rev. *33*, 508–515.

Sztainberg, Y., and Zoghbi, H.Y. (2016). Lessons learned from studying syndromic autism spectrum disorders. Nat. Neurosci. *19*, 1408–1417.

Wilhelm, M., Kukekov, N.V., Schmit, T.L., Biagas, K.V., Sproul, A.A., Gire, S., Maes, M.E., Xu, Z., and Greene, L.A. (2012). Sh3rf2/POSHER protein promotes cell survival by ring-mediated proteasomal degradation of the c-Jun N-terminal kinase scaffold POSH (Plenty of SH3s) protein. J. Biol. Chem. *287*, 2247–2256.

Wöhr, M., Roullet, F.I., Hung, A.Y., Sheng, M., and Crawley, J.N. (2011). Communication impairments in mice lacking Shank1: reduced levels of ultrasonic vocalizations and scent marking behavior. PLoS One *6*, e20631.

Won, H., Lee, H.R., Gee, H.Y., Mah, W., Kim, J.I., Lee, J., Ha, S., Chung, C., Jung, E.S., Cho, Y.S., et al. (2012). Autistic-like social behaviour in Shank2-mutant mice improved by restoring NMDA receptor function. Nature *486*, 261–265.

Yu, X., Qiu, Z., and Zhang, D. (2017). Recent research progress in autism spectrum disorder. Neurosci. Bull. *33*, 125–129.

Yuen, R.K.C., Merico, D., Bookman, M., L Howe, J., Thiruvahindrapuram, B., Patel, R.V., Whitney, J., Deflaux, N., Bingham, J., Wang, Z., et al. (2017). Whole genome sequencing resource identifies 18 new candidate genes for autism spectrum disorder. Nat. Neurosci. *20*, 602–611.

Zhang, H., Kang, E., Wang, Y., Yang, C., Yu, H., Wang, Q., Chen, Z., Zhang, C., Christian, K.M., Song, H., et al. (2016). Brain-specific Crmp2 deletion leads to neuronal development deficits and behavioural impairments in mice. Nat. Commun. *7*, 11773.

Zhou, Q., Homma, K.J., and Poo, M.M. (2004). Shrinkage of dendritic spines associated with long-term depression of hippocampal synapses. Neuron *44*, 749–757.

STAR★METHODS

KEY RESOURCES TABLE

REAGENT or RESOURCE	SOURCE	IDENTIFIER
Antibodies		
GluNR2A	Cell Signaling	Cat#4205; RRID:AB_2112295
GluNR2B	Cell Signaling	Cat#4212; RRID:AB_2112463
GluR1	Epitomics	Cat#3861-1; RRID:AB_10898094
GluR2	Epitomics	Cat#3520-1; RRID:AB_10703317
PSD-95	Abcam	Cat#ab18258; RRID:AB_444362
Beta-actin	Cell Signaling	Cat#3700; RRID:AB_2242334
Synaptophysin	Abcam	Cat#ab8049; RRID:AB_2198854
β-Galactosidase	Abcam	Cat#ab9361; RRID:AB_2198854
NeuN	Abcam	Cat#ab104224; RRID:AB_10711040
GFP	Abcam	Cat#ab13970; RRID:AB_300798
Chemicals		
Lipo2000	Thermo Fisher	Cat#11668019
Tetrodotoxin	Fisheries Science	Li et al., 2017; PMID: 28263300
Picrotoxin	Tocris Bioscience	Cat#1128
D-AP5	Tocris Bioscience	Cat#0106
Experimental Models: Strains		
Mouse: C57/BL6N	Beijing Vital River Laboratory Animal Technology	213
Oligonucleotides		
Southern probe 1-F: 5′-CAAACCTCCTGGGAACCAAGGG-3′	This paper	N/A
Southern probe 1-R: 5′-GACACTGGACTGGCAT CTTATAAAGAAATG-3′	This paper	N/A
Southern probe 2-F: 5′-CTCAAACCAGAATGGAGCAGA-3′	This paper	N/A
Southern probe 2-R: 5′-TCTGTTCGGTGAATACGCTG-3′	This paper	N/A
WT-F: 5′-GCCTCGGATACTGACCTTGCAG-3′	This paper	N/A
WT-R: 5′-CAATCACCTCCAGCACTCTGGT-3′	This paper	N/A
Mutant-F: 5′-GGATCTCATGCTGGAGTTCTTCG-3′	This paper	N/A
Mutant-R: 5′-ACGACCTGCAGCCAAGCTAG-3′	This paper	N/A
Thy1-GFP-F: 5′-TCTGAGTGGCAAAGGACCTTAGG-3′	Life technology	Feng et al., 2000; PMID: 11086982
Thy1-GFP-R: 5′-CGCTGAACTTGTGGCCGTTTACG-3′	Life technology	Feng et al., 2000; PMID: 11086982
Sh3rf2-qPCR-e6/e7-F: 5′-ACAGAGGAGGTGGATAACG-3′	This paper	N/A
Sh3rf2-qPCR-e6/e7-R: 5′-TGGACGAACTGGCATCTT-3′	This paper	N/A
Sh3rf1-qPCR-F: 5′-TGGTGTTTGAGCGTTGCCAGGA-3′	Origene	CAT#: MP215362
Sh3rf1-qPCR-R: 5′-CTTGCTTGACCCGCAGTAGACA-3′	Origene	CAT#: MP215362
Sh3rf3-qPCR-F: 5′-CTCTACCTCCAGTTTGTGCGAC-3′	Origene	CAT#: MP215366
Sh3rf3-qPCR-R: 5′-TGAGGTCACCAGGTTCTTTCCC-3′	Origene	CAT#: MP215366
GAPDH-qPCR-F: 5′-CATCACTGCCACCCAGAAGACTG-3′	Origene	CAT#: MP205604
GAPDH-qPCR-R: 5′-ATGCCAGTGAGCTTCCCGTTCAG-3′	Origene	CAT#: MP205604
Recombinant DNA		
Plasmid: pCDH-CMV-MCS-EF1α-copGFP (pCDH-copGFP)	Generous gift from Dr. Weixiang Guo	N/A
Plasmid: pCDH-coGFP-Sh3rf2	This paper	N/A
Software and Algorithms		
Prism6.0	GraphPad	RRID:SCR_002798
ImageJ	NIH	RRID:SCR_003070

(*Continued on next page*)

Continued

REAGENT or RESOURCE	SOURCE	IDENTIFIER
Imaris 7.6.0	Bitplane	RRID:SCR_007370
SMART Video-tracking	Panlab	RRID:SCR_002852
Avisoft SASLabPro	Avisoft	RRID:SCR_014438
Avisoft-RECORDER	Avisoft	RRID:SCR_014436
Avta Maze software	Anilab	https://www.awn.com/users/anilab
Mini-Analysis 6.0.3	Synaptosoft	http://www.synaptosoft.com/MiniAnalysis/
IBM SPSS Statistics 20	IBM	RRID:SCR_002865
Origin Pro 8	Origin Lab	https://www.originlab.com/

CONTACT FOR REAGENT AND RESOURCE SHARING

Further information and request for resources and reagents should be directed to the Lead Contact, Zhiheng Xu (e-mail: zhxu@genetics.ac.cn).

EXPERIMENTAL MODEL AND SUBJECT DETAILS

Animal studies

All genotypes were produced by mating heterozygous mice. To obtain green fluorescent protein (GFP) labeled neurons, Thy1-GFP line-M transgenic mice in a C57BL6 background (a kind gift from Yi Zuo, Tsinghua University) were interbred with *Sh3rf2*$^{+/-}$ mice to produce GFP$^{+/-}$ / *Sh3rf2*$^{+/+}$, GFP$^{+/-}$ / *Sh3rf2*$^{+/-}$ and GFP$^{+/-}$ / *Sh3rf2*$^{-/-}$ mice. The primers were used for genotyping of GFP sequences are Thy1-GFP-F and Thy1-GFP-R.

Mice were weaned at 22∼24 days of age and housed in groups of 2–5 on a 12 hr light/dark cycle, with free access to food and water except during behavioral testing. All experimental procedures involved were performed according to protocols approved by the Institutional Animal Care and Use Committee at Institute of Genetics and Developmental Biology (IGDB), Chinese Academy of Sciences. All analyses were performed on male littermate mice (Around 26 days old for electrophysiological experiments, at least 8-days-old mice for behavioral studies). All analyses were performed in mice whose genotype was unknown to the experimenter.

METHOD DETAILS

Generation of Sh3rf2 conventional knockout mice

The mouse *Sh3rf2* genomic DNA (10.5 kb) was obtained from a C57BL/6 BAC clone. To disrupt the gene, the targeting vector construct was designed to replace exon1 (excludes 5′UTR) which codes for the first 126 residues (378 bp) with nLacZ-SV40-polyA and the neomycin resistance gene. By this approach, the endogenous translational initiation codon (ATG) was used and reporter gene (nLacZ) was introduced at the same time (Figure S1A). The vector was linearized before electroporation into C57BL/6-derived ES cells. Positive clones were verified by Southern blotting (Figures S1C and S1D) and submitted to blastocyst injection to generate heterozygous Sh3rf2 (*Sh3rf2*$^{+/-}$) mice. F1 offspring were chimeric and were backcrossed to C57BL/6 to allow proper genetic separation of both alleles.

Characterization of *Sh3rf2*$^{+/-}$ mice was carried out by Southern blot analysis. Genomic DNAs obtained from C57BL/6 embryonic stem cells and mice were screened by probe 1 and probe 2 (Figure S1C). The 555-bp Southern probe 1 was generated by PCR using oligonucleotide primers (Southern probe 1-F and Southern probe 1-R). The 531-bp Southern probe 2 was generated by PCR using oligonucleotide primers (Southern probe 2-F and Southern probe 2-R). WT and mutant alleles of mice were confirmed by two sets of genotyping oligonucleotide primers; WT-F and WT-R (PCR product size: 238 bp); mutant-F and mutant-R (PCR product size: 318 bp).

Behavioral tests

All the mice for behavioral tests were housed in groups with 5 mice per cage with the same genotypes. All behavioral tests were performed during the light phase of the cycle between 09:00 and 17:00. All mice were allowed 2 h to habituate to the testing rooms before tests. Experimenters were blind to the genotype when behavioral tests were carried out.

Three-chamber social interaction assay

The three-chamber social interaction assay (Moy et al., 2004; Won et al., 2012) consisted of three phases using a three-chambered apparatus with two small containers (wire cages) in the left or right (not center) chamber, each chamber could be closed and opened with a door. In the first phase, 5–6-week-old WT or *Sh3rf2*$^{+/-}$ mouse was placed in the middle chamber and was allowed to explore the environment freely for 10 min for habituation. The second phase is the social interaction test. In this phase, age-matched WT male

mice were used as Strangers 1 (Stranger mice were habituated to the apparatus by being placed inside wire cages for 25 min each day for 3 days before the test). The WT or *Sh3rf2*$^{+/-}$ mouse was gently guided to the center chamber, and the two entrances to the center chamber were blocked while stranger 1 was introduced into a wire cage in the random side chamber (left or right) and an empty wire cage in the other side chamber. Then, the two entrances were opened to allow the mouse in the center to explore all three chambers freely for 5 min session. Following the 5 min session, the animal was allowed for another 5 min (post-test) to become familiar with the stranger 1 mouse. Following the 10min, in the third phase (social novelty test), the test mouse was gently guided to the center chamber again, with the blockade of the entrances. Stranger 2 was introduced into the previously empty wire cage and again the test mouse was allowed to freely explore all three chambers for a 5 min session. Time spent in each chamber and the test mouse's trajectory were recorded using Avta Maze software.

Free dyadic social interaction

Free social interaction was measured with a novel conspecific as previously described (Feyder et al., 2010). The 5–6-week-old test mouse was acclimated to a clean empty transparent plastic cage for 60 min. Then, an unfamiliar weight-matched male C57BL/6J stimulus mouse (same stimulus mouse not used more than once per day) was then introduced into the cage. The test mouse was allowed to explore the stranger mouse for 10 min. Exploration was defined as each instance in which test mouse tries to sniff the stranger mouse, or orients its nose toward and come close to the stranger as well as aggressive behavior (bite attacks, wrestling). Experiments and analyses were performed on mice whose genotype was unknown to the experimenter.

Nest building assay

The nest building test was performed as previously described with minor modifications (Deacon, 2006). The isolated 5–6-week-old test mice were given one piece of cotton fiber (5 × 5cm) as a nest building material a day before the measurements of nesting behavior. Pictures of the nests were taken 16 hours later. Nesting was scored based on the following score: 1, cotton fiber not noticeably touched (more than 90% intact); 2, cotton fiber partially torn (50%–90% remaining intact); 3, cotton fiber mostly shredded but often no identifiable nest site; 4, an identifiable but flat nest; 5, a (near) well-defined nest with walls.

Olfactory function test

Olfactory processing of both non-social and social scents was assessed based on methods previously described with minor modifications (Feyder et al., 2010). Banana scent and orange scent were used as non-social cues, male urine was used as social cue. 6-7-week-old mice were first habituated to a filter paper which was cut into individual squares (5 cm × 5 cm) and was soaked with tap water into the home cage 3 times for 180 s at a time. Next, mice were exposed to a filter paper soaked in banana scent [about 0.25 mL banana milk drink (Sanyuan)], then orange scent [about 0.25 mL orange juice (Fanta)], and finally male urine [about 0.25 mL collected from at least 7 male C57BL/6J mice, diluted 1:1 with tap water]. Each scent was presented 3 times in succession for 180 s at one time. The time spent sniffing (nose within 2 cm) the filter paper was recorded. Cues were retrieved from the home cage after each session, and inter-session interval was 1 min. The sniffing behavior toward cue-containing filter paper was measured in a blind manner

Ultrasonic vocalization in isolation pulps

This experiment was performed as described previously (Wöhr et al., 2011). Pups of WT or *Sh3rf2*$^{+/-}$ were isolated from their mother and littermates on P8 for 5 min under room temperature. Pups were removed individually from the nest at random and gently placed into an isolation container surrounded by a sound attenuating box. Isolation occurred between 9:00-16:00 during the light phase of the 12:12 h light/dark cycle. Prior to each test, isolation container was cleaned using a 70% ethanol solution, followed by water, and dried with paper towels. USV emission was monitored by an Ultra Sound Gate Condenser Microphone CM16 (Avisoft Bioacoustics, Berlin, Germany) placed approximately 20 cm above the container, the microphone that was used for recording was sensitive to frequencies of 15–180 kHz with a flat frequency response (±6 dB) between 25–140 kHz. USV emission was recorded by Avisoft Recorder software (Version 4.2). For acoustical analysis, recordings were transferred to Avisoft SASLab Pro (Version 5.20) and a fast Fourier transform was conducted (512 FFT length, 100% frame, Hamming window and 75% time window overlap). Correspondingly, the spectrograms were produced at 488 Hz of frequency resolution and 0.512 ms of time resolution. Call detection was provided by an automatic threshold-based algorithm (amplitude threshold: −40 dB) and a hold-time mechanism (hold time: 10 ms). A high-pass filter of 30 kHz and a noise reduction filter of −60 dB were used to reduce noise. Total number of USV, latency to start calling, call duration, peak frequency and peak amplitude were calculated in the automatic parameter analysis for the entire session of 5 min.

Interaction-induced ultrasonic vocalization in adult mice

USV recordings were made with 8-week-old male mice and occurred between 9:00-16:00 h during the light phase of the 12:12 h light/dark cycle. Each male was isolated in a housing cage for at least three days before the recording. On the recording day, the housing cage contained a test mouse were placed in a container surrounded by a sound attenuating box for 30 min. After a 5 min background recording, one randomly chosen C57BL/6J female (5-7 months old, 4-5 mice housed together) was placed in the housing cage to induce courtship USVs in the male mouse. USV emission was monitored by an Ultra Sound Gate Condenser Microphone CM 16 (Avisoft Bioacoustics, Berlin, Germany) placed approximately 20 cm above the housing cage. USV emission was recorded by Avisoft

Recorder software (Version 4.2). For acoustical analysis, recordings were transferred to Avisoft SASLab Pro (Version 5.20) and a fast Fourier transform was conducted (512 FFT length, 100% frame, Hamming window and 75% time window overlap). Correspondingly, the spectrograms were produced at 488 Hz of frequency resolution and 0.512 ms of time resolution. Call detection was provided by an automatic threshold-based algorithm (amplitude threshold: −50 dB) and a hold-time mechanism (hold time: 15 ms). A high-pass filter of 20 kHz and a noise reduction of −60 dB were used to reduce noise. Total number of USV, latency to start calling, call duration, peak frequency and peak amplitude were calculated in the automatic parameter analysis for the entire session of 5 min.

Grooming, digging and jumping in novel cage and home cage

Mice were observed for three kinds of repetitive behaviors based on methods modified from those previously described (Won et al., 2012). The time of grooming and digging or the times of jumping were recorded for a 10 min test in a novel empty cage filled with a thin-layer of clean bedding and then immediately after being returned (individually) back to the home cage with fresh bedding. This procedure was designed to measure repetitive behaviors in both anxiety-provoking and familiar contexts. Jumping was defined as the behavior of a mouse jumps up so that the two hind legs are simultaneously off the ground in the housing cage without cage lid, or jumps outside the cage. Grooming behavior was defined as stroking or scratching of face, head, or body with the two forelimbs, or licking body parts. Digging behavior was defined as the behavior of a mouse where it coordinately uses two fore legs or hind legs to dig out or displace bedding materials.

Rearing in novel cage and home cage

The times of rearing behaviors were recorded for a 10 min test in a novel empty cage filled with a thin-layer of clean bedding and then immediately after being returned (individually) back to the home cage with fresh bedding. This procedure was designed to measure repetitive behaviors in both anxiety-provoking and familiar contexts. Rearing behaviors was defined as the behavior of a mouse puts its weight on its hind legs and extend its head upward with one fore limb or two fore limbs alternatively or coordinately touching the cage wall (Figure S2C, left panel). Rearing without fore limbs was defined as the behavior of a mouse where it stands on its hind legs without support provided by two fore limbs (Figure S2C, right panel).

Marble Burying Test

Use standard and familiar rodent housing cages containing the same and fresh bedding, unscented mouse bedding material to each cage to a depth of 5 cm. Place standard glass toy marbles gently on the surface of the bedding in 4 rows of 5 marbles (Figure S2D). Wash marbles in mild laboratory detergent, rinse exhaustively in distilled-deionized water, and dry prior to each use. Set stop watches or timers for timing session lengths (30 min for each test), then place one mouse into a corner of the cage containing marbles, being careful to place the mouse on bedding as far from marbles as possible, and place the filter-top cover on the cage. Withhold food and water during the test. Allow mouse to remain in the cage undisturbed for 30 min. Task scorers (2-3) blind to the treatment conditions or genotype of the mouse being tested to count the number of marbles buried. Score a marble as buried if two-thirds of its surface area is covered by bedding. Average scores for the number of marbles buried for each mouse.

Analysis of dendritic arborization and spine morphology

In vivo: Thy1-GFP positive age-matched littermates were perfused at 8-week-old. 100 μm coronal sections were cut with a freezing microtome and immunostained with anti-GFP. Slides were individually coded and randomly ordered for image acquisition. Images of dendrite were (random 3 neurons per mouse/ 8 mice for each group) acquired on a Zeiss LSM 700 confocal microscope with a 20 × lense. Images of dendrite spine were acquired on LSM 700 confocal microscope with 100 × 1.4 numerical aperture (NA) lense and 2 x optical zoom. The structure of dendritic fragments and spines was traced and analyzed by 3-D Imaris software. And the classification method of spine morphology is based on the algorithm as followed; mushroom: length (spine) < 3 μm and mean_width (head) ≥ mean_width (neck)x2; stubby: length (spine) < 1 μm; long thin: mean_width (head) ≥ mean_width (neck); filopodia: length (spine) > 2 μm. The investigator was blind to genotype during image acquisition and analysis. *In vitro*: the analyze method is the same as what described above (*In vivo*).

Histological and immunofluorescent staining of Mouse Brain Sections

Animals perfused transcardially with 4% paraformaldehyde (PFA) in 0.1 M phosphate-buffered saline (PBS), pH 7.4. The brains were removed and post-fixed in the same fixative overnight at 4°C. Whole heads from embryos were fixed overnight at 4°C in 4% PFA. Fixed brains were incubated over night at 4°C in 30% sucrose in PBS. 40 μm coronal brain sections were cut with a freezing microtome and washed with PBS for 3 times. For Nissl staining, 40-μm-thick cryostat sections were stained with 0.1% cresyl violet and examined by light microscopy (Nikon) used at room temperature (RT). For immunofluorescent staining, the slices were incubated with blocking buffer at RT for 1 h. Aspirate blocking buffer, added primary antibody diluted in blocking buffer and incubated over night at 4°C. Then washed the slices with PBS for 3 times the next day and incubated 2nd antibody and DAPI diluted in blocking buffer at RT for 1 h. Mounted the slices in anti-fade reagent after washed with PBS. Antibodies used for the immunostaining were β-Galactosidase (chicken, 1:250), GFP (chicken,1:1000).

Biochemical analyses

Hippocampal PSD fractions were prepared from 8-week-old WT, *Sh3rf2*$^{+/-}$ or *Sh3rf2*$^{-/-}$ mice as previously described (Elias et al., 2006). Protein lysate subjected to western blot analysis were separated on SDS-polyacrylamide gel electrophoresis and probed with specific antibodies; NR2A (1:1,000), NR2B (1:1,000), GluR1 (rabbit, 1:1,000), GluR2 (rabbit, 1:1,000), PSD-95 (rabbit, 1:1,000), Beta-actin (mouse,1:1,000), Synaptophysin (mouse,1:1,000). The relative amount of beta-actin was used as loading control. Protein concentrations were measured by the Bradford assay. Enhanced levels of crude postsynaptic membranes from post-nuclear soluble fractions (S1) was detected by enhanced levels of PSD-95 but not synaptophysin (Figure S4C). For quantification, the densitometry measurement of each band (ImageJ) was first normalized to that of Actin and then averaged from at least three independent experiments. Images have been cropped for presentation.

RNA extraction, cDNA synthesis and quantitative real-time PCR

Total RNA was extracted from the brain tissues of WT and *Sh3rf2*$^{+/-}$ mice with TRIzol reagent (life technologies). First-strand cDNA was reversely transcribed with 2 μg total RNA using Go script reverse transcription system (Promega) according to the manufacturer's instructions. Relative transcript levels were measured by qRT-PCR performed in CFX96 real-time system (Bio-Rad) by utilizing Sso Fast EvaGreen Supermix (Bio-Rad). The qRT-PCR program was initiated at 95°C for 30 s, followed by 40 cycles at 95°C for 5 s, 60°C for 30 s. Melting curve analysis was conducted to confirm the specificity of amplification. The specificity of primers was confirmed by BLAST in the mouse transcriptome database (GenBank: NM_001146299.1, NM_172966.3). The PCR products were visualized by staining with ethidium bromide in a 2% agarose gel. The primers used in the qRT-PCR analysis were Sh3rf2-qPCR-e6/e7-F, Sh3rf2-qPCR-e6/e7-R; Sh3rf1-qPCR-F, Sh3rf1-qPCR-R; Sh3rf3-qPCR-F, Sh3rf3-qPCR-R and GAPDH-F, GAPDH-R. All samples were performed in triplicate. The relative RNA expression levels were calculated via a comparative threshold cycle (Ct) method using GAPDH as control: ΔCt = Ct (GAPDH)-Ct (Sh3rf1 / Sh3rf2 / Sh3rf3). The gene expression fold change, normalized to the GAPDH and relative to the mean of control sample, was calculated as $2^{-\Delta\Delta Ct}$.

Primary hippocampal cultures and transfection of primary neurons

Embryonic mice (day E18) were isolated from timed pregnant dams (C57BL/6 or heterozygotes) by cesarean section. Briefly, hippocampal tissue was isolated by microdissection, digested with papain for 15-25 min at 37°C, separated from debris by density gradient centrifugation, and cell number quantified by cell counting chamber. The cells were then plated upon PDL (Sigma-Aldrich) coated 12-mm-diameter glass coverslips, in DMEM medium and 10% heat-inactivated fetal bovine serum. After allowing 2h for the cultures to settle, total medium was replaced with Neurobasal Growth Medium [Neurobasal medium, supplemented with B27, Glutamax, penicillin (10 μg/ml), and streptomycin (10 u/μl)]. The coding sequence (GenBank: NM_001146299.1) of *Sh3rf2* was cloned into the pCDH-CMV-MCS-EF1α-copGFP vector, and then both pCDH-copGFP and pCDH-copGFP-sh3rf2 were transfected into primary neurons. Transient neuronal transfections were performed by lipofection (lipo2000) according to manufacturer's recommendation (life technology).

Electrophysiology

Preparation of hippocampal slices in electrophysiology: Mice at postnatal days 26-31 (P26-31) of the 2 different genotypes (Wild-type and *Sh3rf2*$^{+/-}$) were decapitated after a deep anesthetization by sodium pentobarbital (Nembutal, Abbott, 50mg/kg, i.p.). Their brain was quickly dissected and immediately put into ice-cold oxygenated artificial cerebrospinal fluid (aCSF), which composed of (in mM) 125 NaCl,1.25 $NaH_2PO_4 \cdot 2H_2O$, 2 $CaCl_2 \cdot 2H_2O$, 3 KCl, 2 $MgSO_4$,1.3 Na^+-ascorbate, 0.6 Na^+-pyruvate, 26.2 $NaHCO_3$ and 11 glucose, pH7.4. The coronal hippocampal slices at 300 μm thickness were cut using a vibratome (Leica VT1200S). The slices from the right and left hemispheres were sorted, respectively, and incubated in different places in a chamber filled with oxygenated aCSF at 34°Cfor 30-40 min and then at 20-22°Ctill the use for recording experiments. The animal use strictly followed the protocol that has been approved by the Animal Care and Use Committees of State Key Laboratory of Cognitive Neuroscience and Learning at Beijing Normal University (IACUC-BNU-NKLCNL-2016-02).

Hippocampal slices were transferred to a recording chamber with the perfusion of oxygenated aCSF at a rate of 2 ml/min, and the solution temperature was maintained at 30°C by a temperature controller (TC-324B, Warner Instrument). Whole-cell recording on hippocampal CA1 pyramidal cells (PCs) was performed under an Olympus upright microscopy (BW51WI) equipped with the differential inference contrast (DIC) optics and an infrared video camera (IR-1000). The borosilicate-glass recording micropipettes were pulled by a Sutter puller (P-1000) and filled by an internal solution containing (in mM) 133 K^+-gluconate, 7 KCl, 10 HEPES, 0.4 EGTA, 4 Mg_2ATP, 0.4 Na_2GTP and 10 NA_2-phosphocreatine (pH 7.3; 292 mOsm). The pipette resistance was in a range of 4-5 MΩ. In the experiments of testing neuronal membrane excitability, current-clamp mode was used and step currents (500 ms duration), ranging from 0 to 800 pA with steps of 40 pA, were intracellularly injected to recorded CA1 PCs through the recording pipette to induce action potentials. To record miniature excitatory postsynaptic currents (mEPSCs), PCs were voltage-clamped at −70 mV in the presence of tetrodotoxin (TTX, 0.5 μM), D-AP5 (50 μM) and picrotoxin (20 μM) in the oxygenated aCSF. Recording of mEPSCs normally lasted 30-45 min. Only data from these recordings, in which recorded PCs showed resting membrane potential (Vm) < –65 mV, input resistance (Rin) ≥ 100 MΩ, series resistance (Rs) ≤ 25% of Rin and Rs change < 30% throughout the experiment, were accepted. Electrical signals were filtered at 3 kHz (low pass) and amplified with a MultiClamp 700B (Molecular Devices),

digitalized by a Digidata 1440A converter (Molecular Devices), and acquired at 20 KHz with the PClamp 10.3 (Molecular Devices) into a computer for further analysis. Normally, 2-3 slices from each mouse were used in recording.

QUANTIFICATION AND STATISTICAL ANALYSIS

Information on the statistical tests used, and the exact values of n and what it represents can be found in the Figures or Figure Legends. All data represent means ± standard error of the mean (s.e.m). For two independent data comparisons, unpaired t test, non-parametric Mann-Whitney U test or Kolmogorov–Smirnov test was used to determine statistical significance. *$p < 0.05$, **$p < 0.01$, ***$p < 0.001$. Statistical analyses were performed using GraphPad Prism 6.0 or Microsoft Excel. The analysis of neuronal membrane and spiking properties followed a method described previously (He et al., 2014). The mEPSCs were detected and analyzed using the Mini-Analysis (version 6.0.3).